Final Draft
of the original manuscript:

Plaine, A.H.; Suhuddin, U.F.H.; Alcantara, N.G.; dos Santos, J.F.:
Microstructure and mechanical behavior of friction spot welded AA6181-T4/Ti6Al4V dissimilar joints
In: The International Journal of Advanced Manufacturing Technology (2017) Springer

DOI: 10.1007/s00170-017-0439-2

Microstructure and mechanical behaviour of friction spot welded AA6181-T4/Ti6Al4V dissimilar joint

A. H. Plaine[a,b*], U.F.H. Suhuddin[a], N. G. Alcântara[b], J. F. dos Santos[a]

Affiliation

[a] Helmholtz-Zentrum Geesthacht, Institute of Materials Research, Materials Mechanics, Solid-State Joining Processes, Max-Planck-Str. 1, Geesthacht, Germany.

[b] Federal University of São Carlos, Materials Engineering Department, R. Washington Luís Km 235 - SP 310, Sao Carlos, Brazil.

* Corresponding author: athosplaine@hotmail.com

Abstract

Friction spot welding has become an excellent alternative to produce dissimilar joints in a faster and reliable manner. This paper investigates the microstructure and the mechanical behavior of friction spot welded AA6181-T4/Ti6Al4V dissimilar joints produced by two different tool rotational speeds, 2500 and 3000 rpm, which was previously demonstrated to be the welding parameter with the most influence on the mechanical performance of the joints. Temperature profiles of the joints measured for each welding condition indicated that tool rotational speed directly affects the process temperature and, consequently, the metallurgical reactions taking place at joint interface. Higher temperatures (3000 rpm condition) resulted on a complex and cracked Ti/Al interface related to the local melting of the aluminum plate. In contrast, by decreasing the process temperatures (2500 rpm condition) a continuous $TiAl_3$ reaction layer was formed at Ti/Al interface. Subsequently, the obtained local Von Mises strain distribution of a sound joint were successfully associated with the different stages of a typical force–displacement curve and used to elucidate the fracture evolution under static loading. Moreover, the fatigue behavior of the joints demonstrated that the dissimilar welds exhibited a better performance compared to similar ones.

1. Introduction

Multi-material structures between aluminum and titanium alloys is currently a technologically attractive field of research and their increasing use in the transportation sector for weight and emission reduction is part of the motivation of this study [1]. Aluminum alloys are desirable due to its low density and cost. Titanium

alloys are also promising materials because of their high specific strength and corrosion resistance. Several attempts to join these materials using different traditional fusion welding techniques have been conducted in the past [2-5]. Mainly owing to the formation of brittle intermetallic phases at the interface, these joints are either still limited in performance or too expensive. In this context, mechanical fastening technologies (clinching, riveting, self-piercing riveting) continue to be the most widely used techniques in the automotive and aircraft industries to join dissimilar aluminum and titanium structures. However, these technologies also suffer from a weight penalty, difficulty of automation, requirement for sealants and corrosion problems, creating a niche for new joining techniques [6].

Friction spot welding (FSpW), also known as refill friction stir spot welding, is a solid state joining process developed and patented by Helmholtz-Zentrum Geesthacht (formerly GKSS Forschungszentrum), Germany [7]. In this process, a non-consumable rotating tool consisting of three independently moving parts (pin, sleeve and clamping ring) is used to join materials in a spot-like lap joint configuration. Because of its solid-state character and advantages, such as lower processing time and temperature over conventional fusion welding and geometry compatibility to replace rivets and fasteners, FSpW was widely investigated for joining similar lightweight materials [8-12]. Currently, the main emphasis of FSpW studies has moved a step towards understanding the feasibility of producing dissimilar joints and their process-microstructure-properties correlation [13-16].

Shen et al. [13] discussed the microstructural evolution of dissimilar FSpW joints between AA5086 aluminum alloy and copper. The results showed that a eutectic structure forms near the joint interface, which were detrimental to the joint performance because of its high cracking tendency. Likewise, a large volume of eutectic structure was observed in the weld center of AA5754 and AZ3 dissimilar joints investigated by Suhuddin et. al [17]. In this case, the authors reported that plastic deformation and high-temperature exposure induced both the grain boundary and the interfacial diffusion, thus local melting occurred. During the sleeve retraction period, the “solid–liquid” phase material experienced further diffusion and dynamic recrystallization, resulting in the formation of $Al_{17}Mg_{12}$ intermetallic at the weld center which adversely affected the mechanical properties of the joints. Recently, Plaine et al. [16] investigated the interface formation and properties of friction spot welded joints of AA5754 and Ti6Al4V alloys. The results indicated that a sound interface

depends on an optimum diffusion balance to sufficiently consolidate the joint and to form no excessive intermetallic compounds. In a subsequent work, the authors also investigated the influence of important process parameters on the lap shear strength of FSpW joints applied to the materials proposed in this work, AA6181-T4 aluminum alloy and Ti6Al4V titanium alloy [15]. Produced joints showed good mechanical performance and tool rotational speed demonstrated to be the welding parameter mostly affecting the mechanical performance of the joints. However, there is still a no complete understanding on the influence of this welding parameter on the joint interface microstructure and the fatigue behavior of these joints, a crucial topic for ensuring safe and reliable applications.

This work examines the local interface microstructure of friction spot welded AA6181-T4/Ti6Al4V dissimilar joints produced by different tool rotational speeds. Temperature profiles at the interfacial layers were obtained and associated with the metallurgical reactions. Moreover, the joint presenting the higher ultimate lap shear force was subjected to static and cyclic loads in order to understand its mechanical behavior. These results aim to increase the knowledge of the process-microstructure-properties relationships in dissimilar FSpW joints.

2. Materials and Methods

2.1 Materials

Rolled sheets 1.5 mm thick AA6181-T4 were used in this work. The heat treatment T4 consists of the solutioning of the precipitates in the alloy at high temperatures (515–570 °C) followed by natural aging soon after rolling [18]. The main alloying elements, magnesium and silicon, combine to form the β-Mg_2Si precipitates [19], responsible for the alloy hardening.

Commercial Ti6Al4V sheets with a thickness of 1.5 mm were also used in this study. This alpha-beta alloy is the workhorse alloy of the titanium industry, having a chemical composition of 6% aluminum, 4% vanadium, 0.25% (maximum) iron, 0.2% (maximum) oxygen, and the remainder titanium. Table 1 lists the nominal chemical composition of the materials.

Table 1. Nominal chemical compositions of materials used in this work (wt.%).

Alloys	Ti	Al	Si	Fe	Cu	Mn	Mg	Cr	Zn	V	O
AA6181-T4	0.023	Bal.	0.85	0.25	0.06	0.09	0.74	0.013	0.012	-	-
Ti6Al4V	Bal.	6.25	-	0.14	-	-	-	-	-	3.91	0.12

2.2 Experimental Procedure

FSpW single overlap joints were produced using a RPS200 equipment (Harms & Wende, Germany) with a tool made of molybdenum-vanadium hot work steel. The overlap configuration consisted of the aluminum on top and titanium at the bottom, as schematically shown in Figure 1.

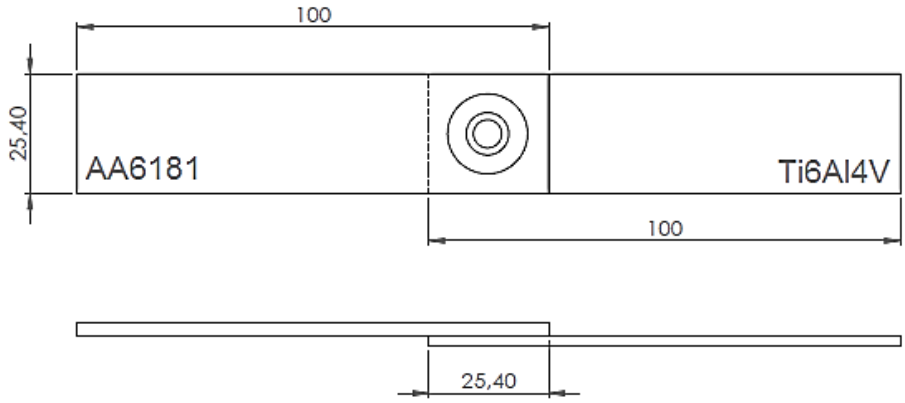

Figure 1. (a) Side view and (b) top view of the overlap joint configuration.

Table 2 lists the joining parameters used in this work, which were selected based on a preliminary study [15] and used to evaluate the influence of tool rotational speed (the parameter with the largest influence on the lap shear strength of the joints) on the process temperatures and, consequently, on the joint interface formation. A digital image correlation system (DIC) – Aramis (GOM, Germany) – was used to monitor the sample strain distribution during the static tests and understand its fracture evolution. Additionally, temperature measurements were carried out using K-type thermocouples embedded in three different positions of the joint interface, as illustrated in Figure 2.

Table 2. FSpW process parameters used in this work.

Condition	Rotational Speed (rpm)	Dwell Time (s)	Plunge Depth (mm)	Clamping Force (kN)
1	2500	3	1.4	12
2	3000	3	1.4	12

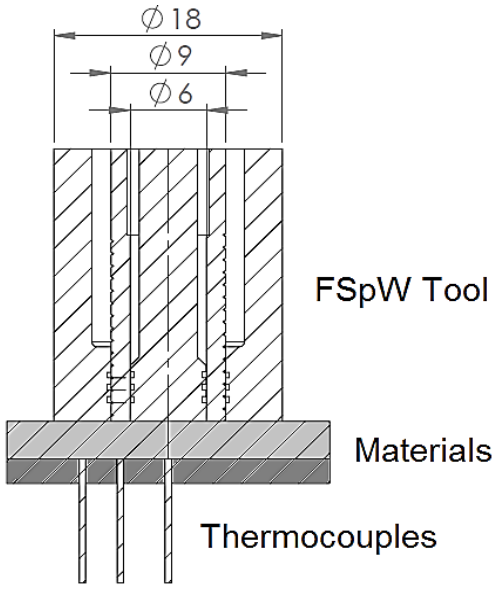

Figure 2. A schematic illustration of the thermocouple placement during the temperature measurements.

2.3 Microstructural analysis

The cross-section of the joints was analyzed using an optical microscope (DM IR microscope, Leica) under reflective light and a FEI Quanta 650 scanning electron microscope fitted with EDAX energy dispersive X-ray spectrometer (EDS) detector. The joints were previously cut close to the middle of the spot using a low-speed saw with diamond blade and embedded in cold curing epoxy resin followed by standard grinding and polishing procedures.

2.4 Fatigue Testing

Fatigue tests were performed for the best welding condition (with the highest ultimate lap shear force) using a Schenck servo-hydraulic testing system at five different load amplitudes. A load ratio of R (Pmin/Pmax) equal to 0.1, a sinusoidal wave form, and a frequency of 20Hz were applied for all the tests. For higher accuracy seven specimens were tested at each stress level.

The two-parameter Weibull distribution was used to analyze the probability aspects of the fatigue results. It is also being used to model extreme values such as failure times and fatigue life. The probability density function (PDF) - the most known definition of two-parameter Weibull distribution - has been indicated in the following Eq. (1).

$$f(x) = \frac{\beta}{\alpha}(x\alpha)^{\beta-1}\, e^{-(\frac{x}{\alpha})^{\beta}} \qquad \alpha \geqslant 0, \beta \geqslant 0 \tag{1}$$

where α and β is the scale (characteristic life) and shape parameters, respectively [20].

If PDF equation is integrated, the cumulative density function (CDF) is obtained, Eq. (2).

$$F_f(x) = 1 - e^{-\left(\frac{x}{\alpha}\right)^{\beta}} \quad (2)$$

After computing the Weibull parameters α and β obtained in the Weibull plot, it is possible to compute the Weibull mean life or mean time to failure, which represents the expected life for a given stress amplitude for fatigue testing. Hence,

$$\text{MTTF} = \alpha\Gamma\left(1 + \frac{1}{\beta}\right) \quad (3)$$

where Γ is the gamma function [21].

3. Results

3.1. Process temperature

Figure 3 and Figure 4 present the process temperature profiles of two FSpW joints produced with different tool rotational speeds, 2500 rpm and 3000 rpm, having an ultimate lap shear force of 6449 ± 554 N and 4910 ± 249 N, respectively [15]. According to the results, tool rotational speed plays an important role in the amount of the total heat input applied during the process as it directly affects its temperature. It was also observed that for both welding conditions, the interfacial temperatures under the pin (weld center) are slightly higher than the temperatures under the sleeve. Moreover, an increasing of rotational speed from 2500 to 3000 rpm causes a temperature rise in the peak temperature at the weld center from 540 °C to 582 °C (corresponding to 84% and 90%, respectively, of the incipient melting point of the AA6181-T4 [22]). It might be argued that the tool rotational speed values used in the present work is excessively high for solid state processes involving aluminum alloys. However, the literature reports that tool rotational speeds from 2000 to 3000 rpm are required during Al alloy friction spot welding to provide sufficient heat input in a short spot welding cycle in order to achieve acceptable joint strength properties [8]. Since joining time was not altered by the tool rotational speed variation, the degradation of the mechanical properties with increasing tool rotational speed could be possibly

associated with a greater amount of intermetallic compounds formed at the joint interface, exclusively associated with an increase of the atoms diffusion flux.

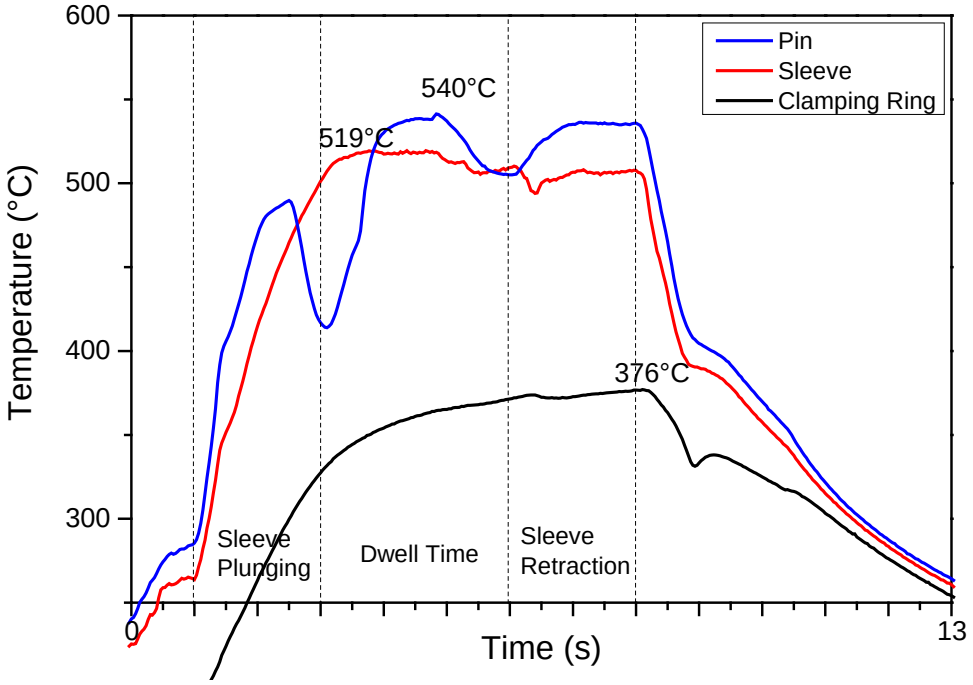

Figure 3. Process temperature profile of the joint produced with a tool rotational speed of 2500 rpm.

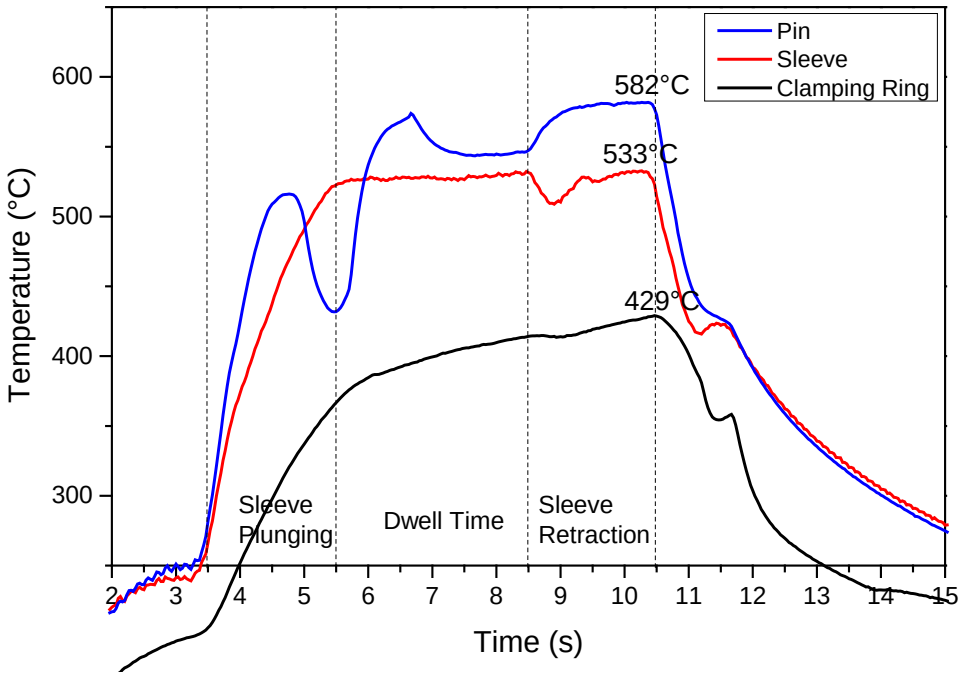

Figure 4. Process temperature profile of the joint produced with a tool rotational speed of 3000 rpm.

3.2. Microstructural features

Figure 5(a) illustrates a top view of a representative AA6181-T4 and Ti6Al4V joint, showing that FSpW process provides good surface finishing with a smooth and keyhole free surface. The cross-sectional view of the joint is also shown in Figure 5(b). No defects or obvious reductions of thickness were observed in the weld. The flat interface between the joining parts demonstrates that no mechanical interlocking contributes to the joint strength under shear loading, indicating that the bonding mechanism is only related to the metallurgical reactions at the joint interface.

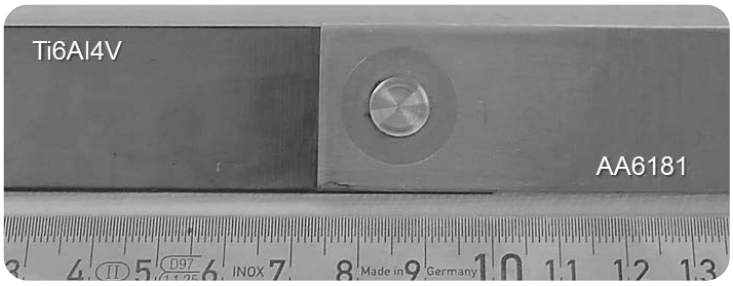

(a)

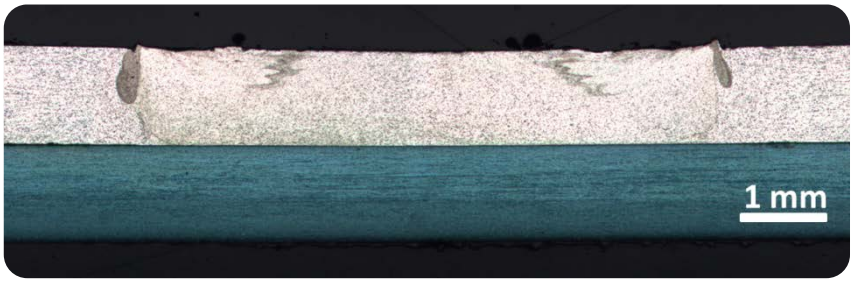

(b)

Figure 5. (a) Representative top view and (b) mid cross-section micrograph of the AA6181/Ti6Al4V joint.

Microstructure details of the Ti/Al interface welded with the lowest RS is shown in Figure 6. Despite the short reaction time for the elements to interdiffuse, intermetallic compounds were formed during welding process, especially close to the weld center. At this region, a continuous reaction layer with width of about 0.8 μm is observed adjacent to the Ti/Al interface. EDS results indicated that the reaction layer is composed of $TiAl_3$. In addition, according to the composition profile showed in the inset of Figure 6(a), it was found some Si dissolved in the TiAl3 layer (approximately 10%). The Si content had a slight decrease across the TiAl3 layers from the region near the Al side to the region near the Ti side. Pang et al. [23] investigated the effect of solid solution of Si on the mechanical properties of $TiAl_3$, showing that the Si leads

to an increasing on the elastic modulus and hardness of the TiAl3 layer compared to the pure TiAl3. In addition, it results in a reduced plasticity.

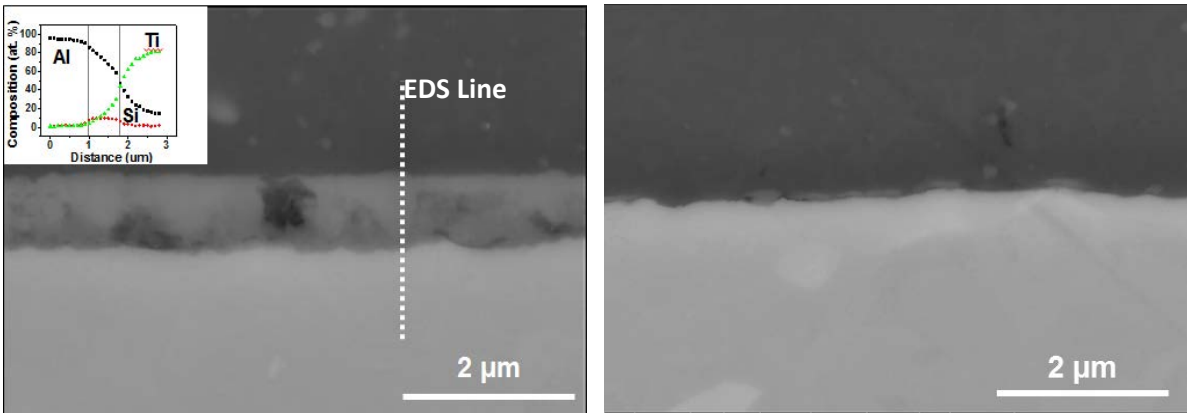

(a) (b)

Figure 6. SEM micrographs of the joint interface produced with a tool RS of 2500 rpm joint interface (a) under the pin (weld center), with the inset of the energy-dispersive X-ray spectroscopy concentration profile along EDS line of the image, and (b) under the sleeve.

According to Ti–Al binary phase diagram [24], Ti and Al reactions take place only at temperatures over 665 °C. Nevertheless, the FSpW joints have been able to form intermetallic compounds at unfavorable conditions, within temperatures lower than 600 °C. It is well known that friction-based joining process possess a stir zone with a high density of low-angle grain boundaries and a fine grain structure due to the intense plastic deformation and the process temperatures [25]. These conditions results on a more open structure, thereby allowing for lower activation energy for diffusion. Also, the surface diffusion is known to occur much faster than lattice diffusion. Therefore, the diffusion rate during friction based processes must be higher compared to other welding processes, as confirmed by Yashan et al. [26] in a previous study on friction welding of AISI 316 stainless steel.

Figure 7 shows the microstructure of the Ti/Al interface with the highest RS. A complex and cracked interfacial reaction layers were formed near to the Ti/Al interface, where it was even possible to observe the presence of a dendritic structure characteristic of solidification phenomenon. The average width of the interfacial reaction layers was approximately 2 µm. In order to identify the interface, a compositional mapping of the main elements was carried out by EDS, as shown in Figure 8.

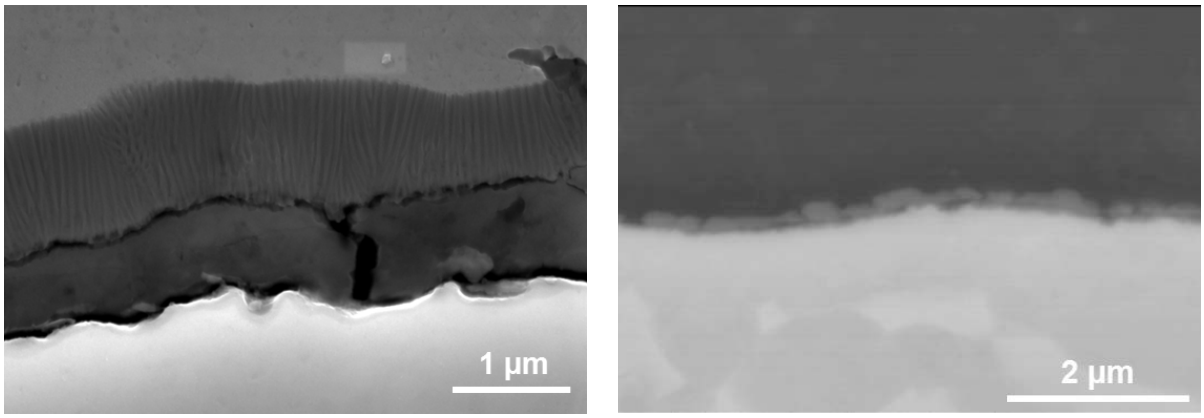

(a) (b)

Figure 7. SEM micrographs of joint interface produced with a tool RS of 3000 rpm (a) under the pin (weld center) and (b) under the sleeve.

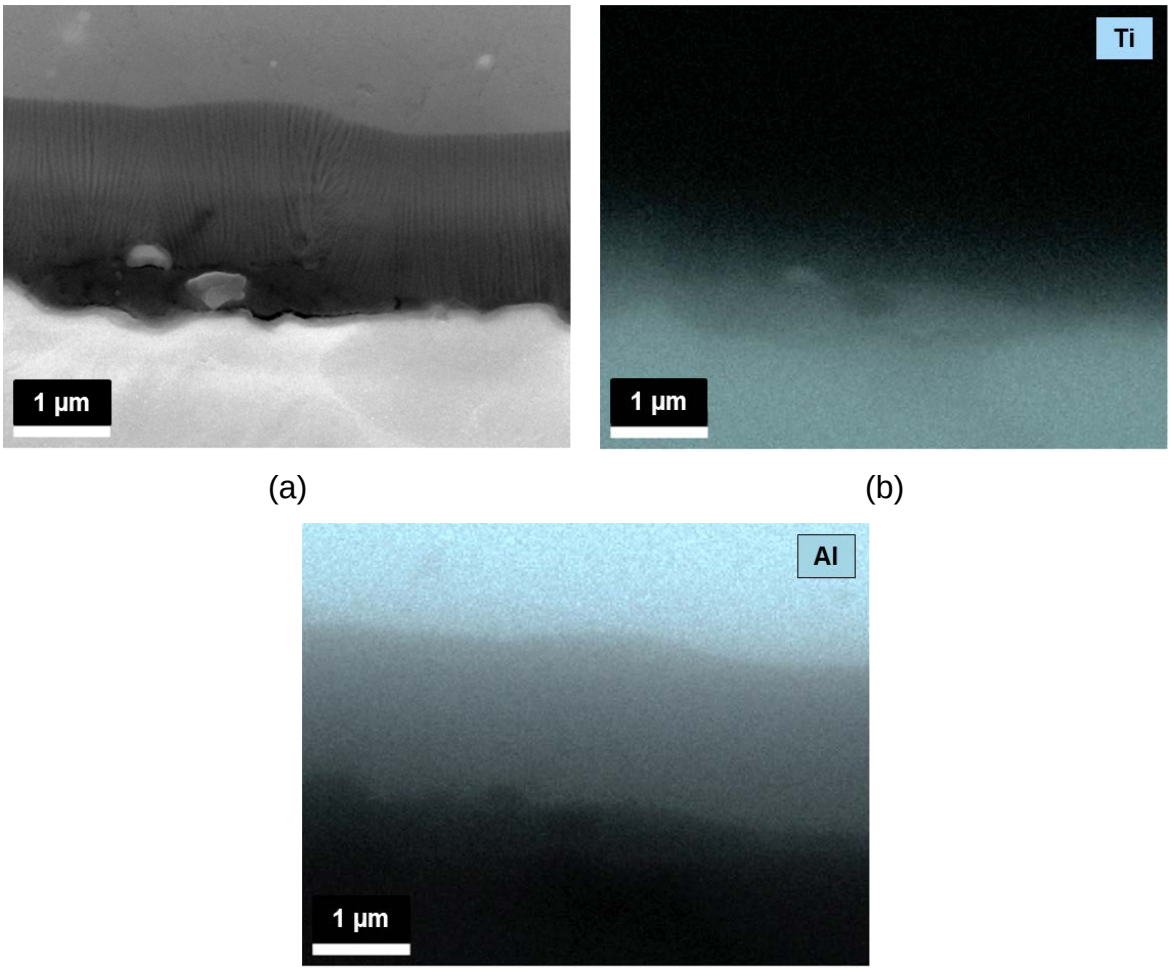

(a) (b)

(c)

Figure 8. SEM micrograph of the joint interface produced with a tool RS of 3000 rpm (a) under the pin and its EDS elemental mapping of (b) Ti-K and (c) Al-K.

According to the results, the joint interface seems to occur in different stages. Initially, Ti–Al intermetallics such as $TiAl_3$ were formed near the Ti/Al interface, as previously discussed. Differential thermal analysis reveal that the reaction between Ti and Al is a significant exothermal process which promotes the Al depletion near the α-Al/intermetallic interface (see Figure 8(c)) and could lead to the local Al melt [27]. At the same time, owing to the concentration gradient and flowing of weld metal, a number of Si atoms might be diffused from the molten pool to the liquid–solid interface. According to Al–Si binary phase diagram [28], α-Al grains with a small dissolution of Si started to crystallize firstly during cooling process, resulting in an epitaxial growth of columnar dendrites towards the unmelted portion of the aluminum plate (base material). These findings suggest that local melting might occur when abnormally high (some believe unacceptably high) tool rotational speed settings are used during friction spot welding operations.

3.3. Global mechanical properties

3.3.1. Behaviour of dissimilar FSpW joints subject to static loading

Friction spot welded AA6181/Ti6Al4V dissimilar joints were subject to single lap shear testing, as shown in [15]. For overlap joints of materials with different stiffness, the forces cause a secondary bending moment, as shown in Figure 9(a). The secondary bending and the pulling forces create a stress concentration at the notch tip of the interface (red circle). In order to better understand the mechanical behavior of the AA6181-T4/Ti6Al4V joints under lap shear, DIC measurements of local Von Mises strain distribution (Figure 9(b)) were associated with stages of a typical force–displacement curve for a sound FSpW joint (Figure 9(c)).

(a)

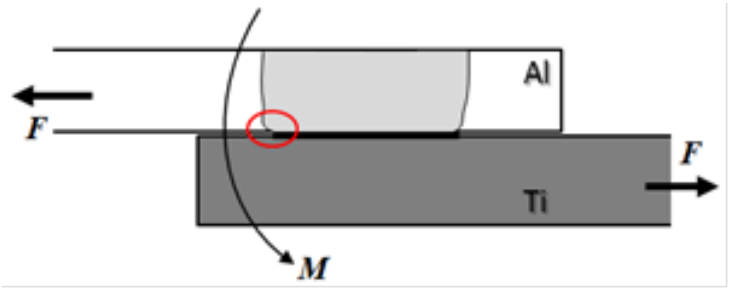

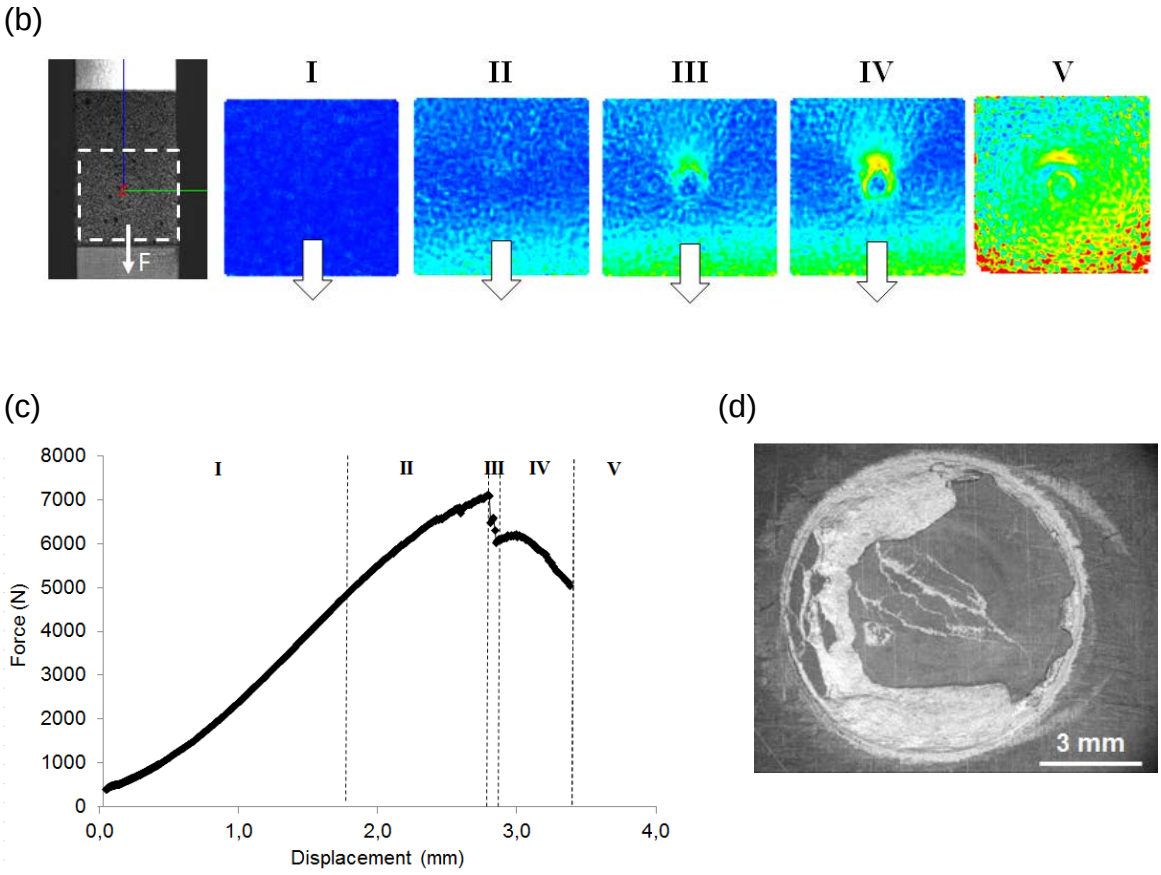

Figure 9. Single lap shear testing of an AA6181-T4/Ti6Al4V FSpW joint: (a) schematic drawing of the main forces acting on the joint, and crack nucleation and propagation points; (b) Von Mises strain distribution at the specimen surface during stages of the test; (c) typical force–displacement curve; (d) fracture surface.

The force–displacement curve first shows an elastic behavior (Stage I). As the load increases, an opening between the plates (due to the secondary bending of the specimen during the test) is initiated and the strain is concentrated around the spot joint (Stage II). At this point a stress component perpendicular to the interface arises and some annular cracks start to nucleate to propagate around the joint into the aluminum plate towards the weld center. Thereafter, the brittle intermetallic layer fracture catastrophically as the perpendicular stresses reach a critical level, resulting in an instantaneous decrease in force (Stage III). In Stage IV, the cracks continue propagating and reach a point where the stresses acting in the remaining interface can no longer sustain the load and it fails (Stage V). The observed strain distribution

is in agreement with a previous numerical model developed to lap shear specimens of FSpW joints [9].

3.3. Behaviour of dissimilar FSpW joints subject to cyclic loading

Fatigue testing was performed to evaluate the joint behavior subjected to fluctuating stresses. Table 3 shows the five different load percentages of the maximum lap shear load, corresponding stresses, fatigue life and failure mode. Because of the limited operation time of the testing machine, some tests were terminated manually as their cycles were beyond 5.0 x10^6 cycles.

Table 3 Results of fatigue tests for FSpW specimens.

Load (%)	S_{max} (MPa)	S_{min} (MPa)	S_a (MPa)	Cycles (N_f)	Failure Mode*
10	22.2	2.2	20.0	>50000000	-
				>50000000	-
				>50000000	-
				>50000000	-
				>50000000	-
				>50000000	-
				>50000000	-
12.5	29.6	3.0	26.6	603452	TW
				474024	TW
				685233	TW
				748637	TW
				524531	TW
				713592	TW
				596331	TW
15	37	3.7	33.3	156091	TW
				183314	TW
				104088	TW
				226992	TW
				143855	TW
				188961	TW
				200563	TW
20	51.9	5.2	46.7	88363	TW
				50637	TW
				23237	TW
				37422	TW
				68952	TW
				32004	TW
				78523	TW
25	59.3	5.9	53.4	9517	TW
				13228	TW
				17614	TW
				20125	TW
				12288	TW
				10862	TW
				11584	TW

* TW – through weld failure

Figure 10 shows the Weibull plot for the different load condition. However, since none of the samples tested for 10% of the maximum load failed, this data has not been used further in the analysis. Recurring to the graph, it is possible to obtain the values of the Weibull slope (β) and characteristic life (α) by linear regression. Table 4 shows the values of α and β for each stress level, as well as the Weibull mean life (obtained from Eq. (3)).

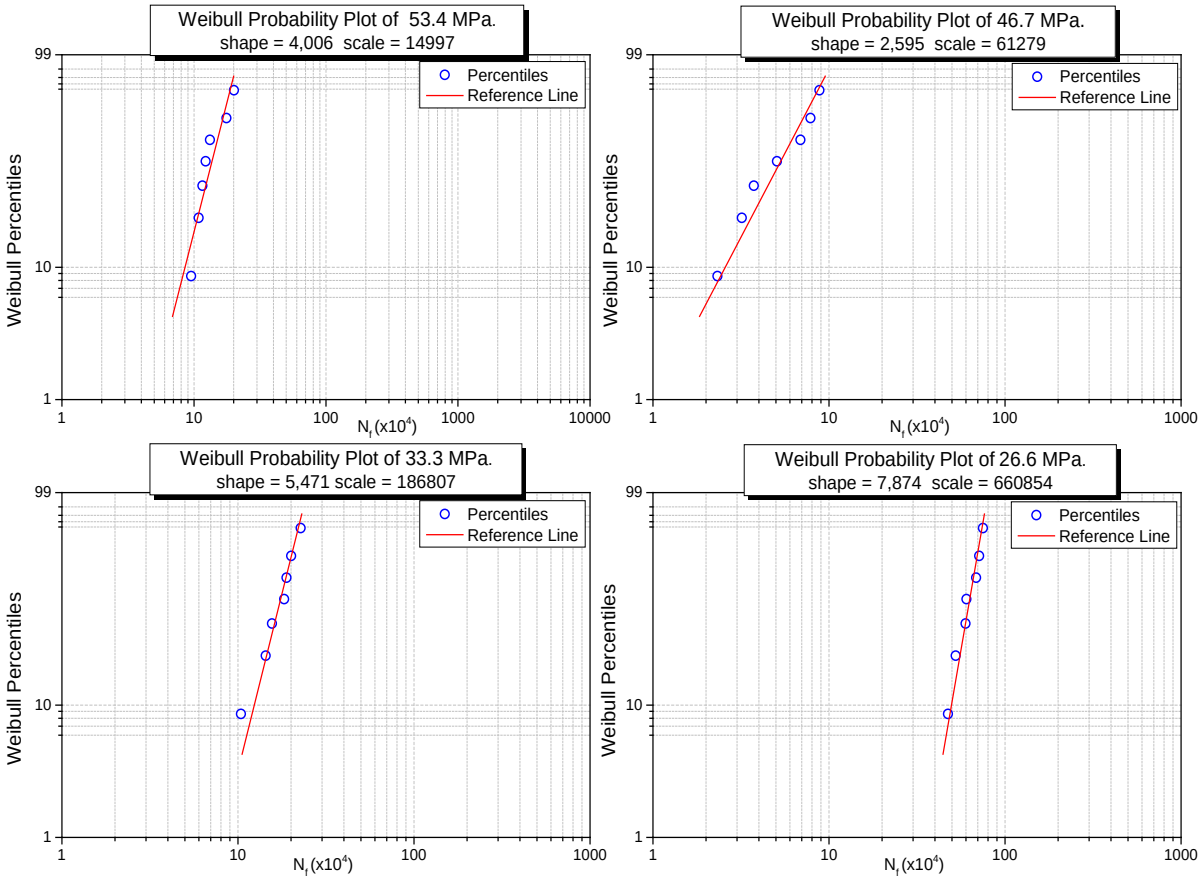

Figure 10. Weibull plots for the tested stress amplitudes.

Table 4 Weibull parameters and mean life for each stress amplitude.

S_a (Mpa)	Scale parameter (α)	Shape parameter (β)	Weibull mean life (cycles)
26.6	660854	7.874	621873
33.3	186807	5.471	172408
46.7	61279	2.595	54426
53.4	14997	4.006	13595

The S–N curve obtained for the Weibull mean fatigue life is shown in Figure 11. Power function has been used in Eq. (4) for the evaluation of fatigue test data [29, 30]. This equation is valid for fatigue lives that are within the range of $1x10^3$ –

$5x10^8$ cycles for non-ferrous metals such as aluminum and titanium [30]. Based on the results, a fatigue limit of 22 MPa (12% of the maximum average static fracture load) was determined for the AA6181/Ti6Al4V joints produced by FSpW. Recently, Effertz et. al. [12] evaluated the fatigue behavior of friction spot welded 7050-T76 aluminium alloy, showing a fatigue limit corresponding to only 10% of the ultimate lap shear force. The better performance of the dissimilar joints can be attributed to the process parameters optimization as it reduced the formation of IMC in the joint interface [15] and to the absence of the typical hook profile at the joint interface - a geometric defect that adversely affect the joint strength [31].

$$S_a = a \times (N_f)^b \quad (4)$$

where Sa is the stress amplitude, Nf the number of cycles and a and b are constants

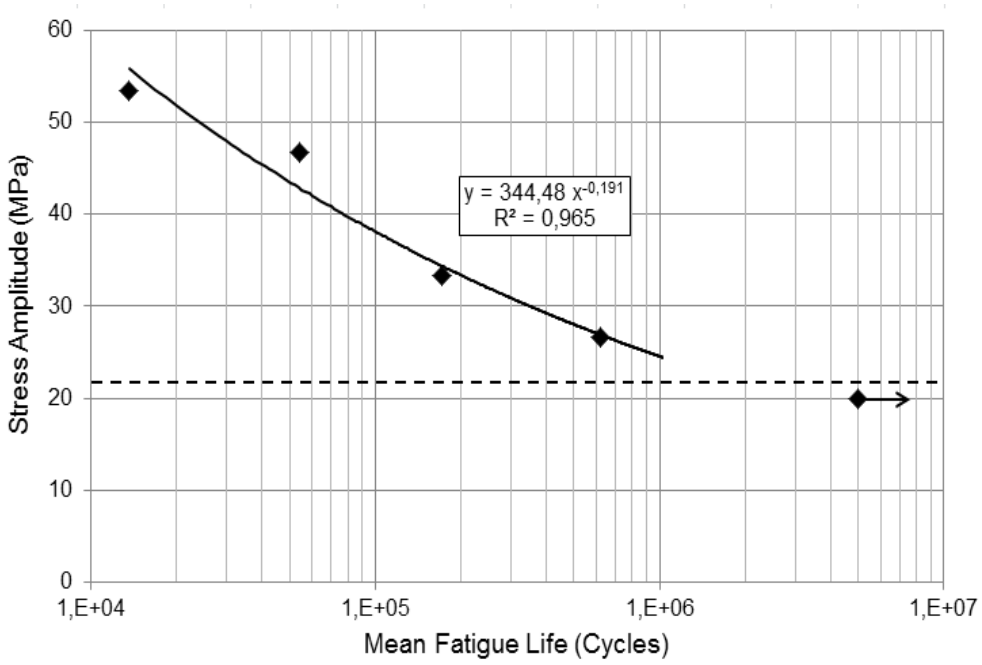

Figure 11. *S–N* curve of Ti/Al dissimilar joints produced by FSpW.

Figure 12 shows details of the interfacial fracture surface morphology at the titanium side, showing the same fracture mode observed in the lap shear specimen. The image confirms that the primary fatigue crack initiates at the notch of the spot weld and propagates around the weld and towards its center. The fatigue crack propagation with its advancing direction indicated by the dashed arrows in Figure 12(a) was characterized by fatigue striations (Figure 12(b)). The more centralized

area consists of deformed dimples (Figure 12(c)), indicating the remaining joint area previous to the final fracture.

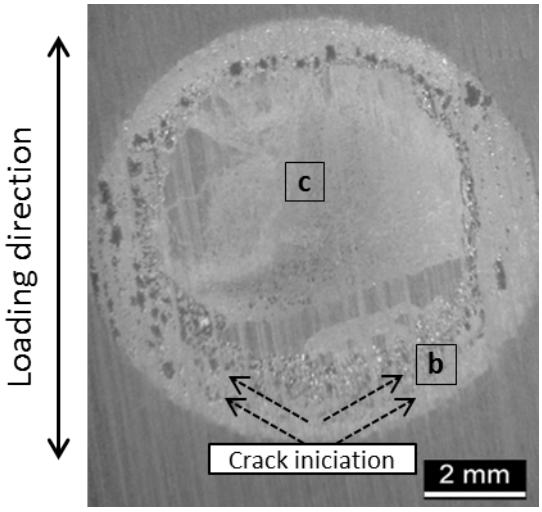

(a)

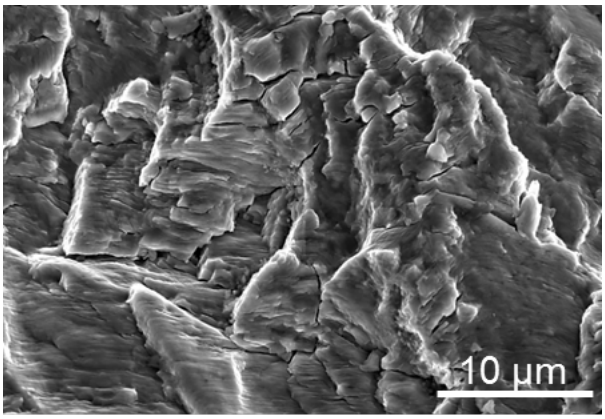

(b)

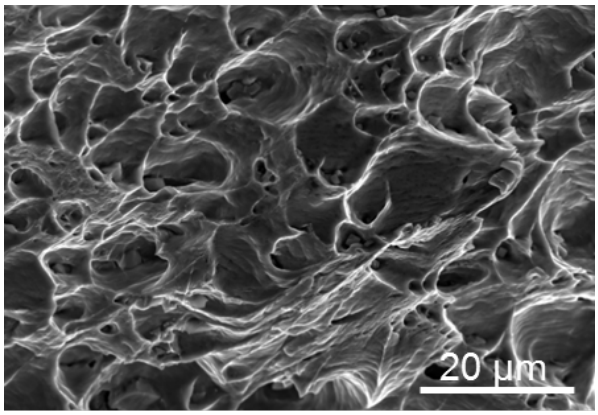

(c)

Figure 12. Macroscopic and SEM images of the fatigue fracture surface an AA6181-T4/Ti6Al4V FSpW joint: (a) general fracture surface overview showing the primary crack initiation and propagation area; (b) and (c) high magnification images showing, respectively, fatigue striations in the crack propagation area and deformed dimples in the final fracture area.

4. Conclusions

Friction spot joints of aluminum alloy AA6181-T4 and titanium alloy Ti6Al4V produced by two different tool rotational speeds were investigated regarding their microstructure and mechanical behavior. The flat interface between the joining parts demonstrated that the interfacial layer formed between the plates is the only bonding mechanism of these joints. A decreasing on ultimate lap shear force with increasing

tool rotational speed were observed and associated with the local melting of the aluminum plate, resulting on a complex and cracked joint interface. Oppositely, with a lower rotational speed, a continuous and tiny reaction layer with width of about 0.8 μm was formed at Ti/Al interface. Measurements of the Von Mises strain distribution were successfully used to understand the fracture evolution of the best welding condition (at 2500 rpm) under static loading, showing that the cracks nucleates at the notch tip of the interface between the two sheets and propagates towards the weld center. Additionally, the referred dissimilar joints presented a fatigue strength slightly higher compared to similar aluminum FSpW joints, which could be related to the small amount of IMC formed at the reaction layer and also to the absence of geometric features like the typical hook profile.

Acknowledgments

The authors would like to acknowledge the financial support received from CNPq (National Council for Scientific and Technological Development - Brazil)

References

1. Lehmhus, D.B., M. ; Herrmann, A. ; Kayvantash, K., Structural Materials and Processes in Transportation. John Wiley & Sons. 2013: Wiley-VCH Verlag GmbH & Co KGaA. 500.
2. Chang, S.Y., et al., Brazing of 6061 aluminum alloy/Ti–6Al–4V using Al–Si–Cu–Ge filler metals. Journal of Materials Processing Technology, 2012. 212(1): p. 8-14.
3. Vaidya, W.V., et al., Improving interfacial properties of a laser beam welded dissimilar joint of aluminium AA6056 and titanium Ti6Al4V for aeronautical applications. Journal of Materials Science, 2010. 45(22): p. 6242-6254.
4. Song, Z., et al., Interfacial microstructure and mechanical property of Ti6Al4V/A6061 dissimilar joint by direct laser brazing without filler metal and groove. Materials Science and Engineering: A, 2013. 560: p. 111-120.
5. Qiu, R., et al., Characterization of joint between titanium and aluminum alloy welded by resistance spot welding with cover plate. QUARTERLY JOURNAL OF THE JAPAN WELDING SOCIETY, 2009. 27(2): p. 109s-113s.
6. Wu, A., et al., Interface and properties of the friction stir welded joints of titanium alloy Ti6Al4V with aluminum alloy 6061. Materials & Design, 2015. 71: p. 85-92.
7. Schilling, C.D.S., J.;, Method and Device for Linking at Least Two Adjoining Work Pieces by Friction Welding., G.F.G. Gmbh, Editor. 2001.
8. Rosendo, T., et al., Mechanical and microstructural investigation of friction spot welded AA6181-T4 aluminium alloy. Materials & Design, 2011. 32(3): p. 1094-1100.
9. Mazzaferro, J.A.E., et al., Preliminary study on the mechanical behavior of friction spot welds. Soldagem & Inspeção, 2009. 14: p. 238-247.
10. Campanelli, L.C., et al., Metallurgy and mechanical performance of AZ31 magnesium alloy friction spot welds. Journal of Materials Processing Technology, 2013. 213(4): p. 515-521.
11. Oliveira, P.H.F., et al., Preliminary study on the feasibility of friction spot welding in PMMA. Materials Letters, 2010. 64(19): p. 2098-2101.

12. Effertz, P.S., et al., Fatigue life assessment of friction spot welded 7050-T76 aluminium alloy using Weibull distribution. International Journal of Fatigue, 2016. 87: p. 381-390.

13. Shen, Z., et al., Microstructure and mechanical properties of friction spot welded 6061-T4 aluminum alloy. Materials & Design, 2014. 54: p. 766-778.

14. Suhuddin, U., et al., Microstructure and mechanical properties of friction spot welds of dissimilar AA5754 Al and AZ31 Mg alloys. Materials Science and Engineering: A, 2014. 590: p. 384-389.

15. Plaine, A.H., et al., The optimization of friction spot welding process parameters in AA6181-T4 and Ti6Al4V dissimilar joints. Materials & Design, 2015. 83: p. 36-41.

16. Plaine, A.H., et al., Interface formation and properties of friction spot welded joints of AA5754 and Ti6Al4V alloys. Materials & Design, 2016. 93: p. 224-231.

17. Suhuddin, U.F.H., V. Fischer, and J.F. dos Santos, The thermal cycle during the dissimilar friction spot welding of aluminum and magnesium alloy. Scripta Materialia, 2013. 68(1): p. 87-90.

18. Heat Treating, in ASM Handbook. 1991.

19. Milkereit, B., et al., Continuous cooling precipitation diagrams of Al–Mg–Si alloys. Materials Science and Engineering: A, 2012. 550: p. 87-96.

20. Zhao, Y.X. and H.B. Liu, Weibull modeling of the probabilistic S–N curves for rolling contact fatigue. International Journal of Fatigue, 2014. 66: p. 47-54.

21. Sakin, R. and İ. Ay, Statistical analysis of bending fatigue life data using Weibull distribution in glass-fiber reinforced polyester composites. Materials & Design, 2008. 29(6): p. 1170-1181.

22. Totten, G.E. and D.S. MacKenzie, Handbook of Aluminum: Vol. 1: Physical Metallurgy and Processes. 2003: CRC Press.

23. Pang, J.C., et al., Effect of solid solution of Si on mechanical properties of TiAl3 based on the multi-laminated Ti-(SiCP/Al) composite system. Materials Science and Engineering: A, 2013. 579(0): p. 57-63.

24. Sujata, M., S. Bhargava, and S. Sangal, On the formation of TiAl3 during reaction between solid Ti and liquid Al. Journal of Materials Science Letters. 16(13): p. 1175-1178.

25. Suhuddin, U.F.H.R., et al., Grain structure evolution during friction-stir welding of AZ31 magnesium alloy. Acta Materialia, 2009. 57(18): p. 5406-5418.

26. Yashan, D., et al., Inertia friction welding of 1100 aluminum to type 316 stainless steel. Welding Journal (Miami, Fla), 1987. 66(8): p. 27-37.

27. Shouzheng, W., et al., Microstructure and joining mechanism of Ti/Al dissimilar joint by pulsed gas metal arc welding. The International Journal of Advanced Manufacturing Technology, 2014. 70(5): p. 1137-1142.

28. Hansen, S.C. and C.R. Loper, Effect of antimony on the phase equilibrium of binary Al□Si alloys. Calphad, 2000. 24(3): p. 339-352.

29. Khashaba, U.A., Fatigue and Reliability Analysis of Unidirectional GFRP Composites under Rotating Bending Loads. Journal of Composite Materials, 2003. 37(4): p. 317-331.

30. Vidal, C., V. Infante, and P. Vilaça, Assessment of improvement techniques effect on fatigue behaviour of friction stir welded aerospace aluminium alloys. Procedia Engineering, 2010. 2(1): p. 1605-1616.

31. Cao, J.Y., et al., Hook formation and mechanical properties of friction spot welding in alloy 6061-T6. Journal of Materials Processing Technology, 2016. 230: p. 254-262.